JOURNAL OF MATERIALS SCIENCE, 30, (1995) 2382–2389

Effect of particle size distribution on sintering

Part II *Sintering of alumina*

J.-M. TING* and R.Y. LIN
Department of Material Sciences and Engineering, University of Cincinnati, Cincinnati, OH 45219, USA

A sintering model, taking into account the effect of particle size distribution and the effect of grain growth, was developed previously. Experimental data from the sintering of high-purity alumina were used to testify this model. The sintering was carried out at 1500 °C in air for various lengths of time. The results agreed with the prediction of the model. The powders with a narrower starting particle size distribution exhibited a lower sintering rate prior to the occurrence of grain growth, but a higher densification rate after the grain growth took place. The grain size/density trajectory was applied to reveal the effect of particle size distribution on sintering behaviour. It is suggested that powders with a narrower size distribution are preferable.

1. Introduction

In a previous paper [1], the shrinkage of powder compact prior to the occurrence of grain growth was derived and can be expressed

$$R = \int K_1 \frac{t^n}{G^{m_0}} f(G)\,dG \Big/ \int f(G)\,dG = K_1 t^n F_0(G) \tag{1}$$

where K_1, m_0, and n are constants, and $F_0(G)$ denotes the rate factor of shrinkage before the occurrence of grain growth and depends on the characteristics of size distribution. After grain growth takes place, the sintering equation becomes

$$R = \int\int K_2 \frac{1}{G^{m_1}}\left(\frac{1}{G_g} - \frac{1}{G}\right) f(G)\,h(t)\,dG\,dt \Big/ \int f(G)\,dG = K_2 H(t)\,F_1(G) \tag{2}$$

with

$$H(t) = \int h(t)\,dt \tag{2a}$$

$$F_1(G) = \int \frac{1}{G^{m_1}}\left(\frac{1}{G_g} - \frac{1}{G}\right) f(G)\,dG \tag{2b}$$

where K_2 and m_1 are constants, and $F_1(G)$ denotes the rate factor after grain growth takes place. From these two equations the effect of particle size distribution on sintering kinetics can be obtained by performing integrations to obtain $F_0(G)$ and $F_1(G)$. These equations predict a dependence of densification on the width of particle size distribution. Prior to the occurrence of grain growth, densification rate exhibits a peak value as the starting particle size distribution width increases. When grain growth occurs, densification rate decreases as the distribution width increases. In the present paper, experiments on the sintering of alumina were carried out to verify the prediction of the modelling.

2. Experimental procedure

Three types of alumina powders from the CERALOX Corporation (Tucson, Arizona, USA) were used in this study. The difference between these powder types is the powder size distribution. These powders were selected such that there were powders differing from each other in the median size (Material 1 versus Material 2) and in the width of distribution (Material 1 versus Material 3). The characteristics of these powders, supplied by the manufacturer, are given in Table I.

TABLE I Parameters showing the powder size characteristics

Powder	Material 1	Material 2	Material 3
G_g	0.50	0.98	0.50
σ_g	2.04	2.52	1.72
Mg (ppm)	297	306	324
Na (ppm)	30	27	17
Si (ppm)	22	25	18
Fe (ppm)	13	15	16
Ca (ppm)	9	8	11
Others (ppm)	< 15	< 10	< 10

* *Present address*: Applied Sciences, Inc., P.O. Box 579, Cedarville, OH 45314-0579 USA.

0022–2461

The powders were dry blended and compressed in a single-action, cylindrical press die at 51.7 MPa (7500 p.s.i.) to 68.9 MPa (10 000 psi). The average green density is about 55 to 56% of that of theoretical density. Five as-pressed pellets of each kind were placed together in a high-purity alumina crucible and embedded with powders of the same type. The sintering was carried out at 1500 °C in air. The temperature in the hot zone was kept constant to within ± 1 °C. The crucible was inserted into or removed from the hot zone in approximately 1.5 min. The specimens were heated to the desired temperature 5 min after the specimens were located in the hot zone. This time was taken as the initial time for the isothermal sintering. The sintering time ranged from 5 to 235 min. After the sintering, the Archimedes method was applied to determine the density of each specimen. The volume shrinkage was then calculated from the density data. For microstructural analysis, the specimens were sectioned by a diamond saw, polished by diamond pastes and thermally etched at 1300 °C for 30 min in air. The etched specimens were then examined using scanning electron microscopy (SEM). To determine the grain size distributions, an image analysis station was used to measure grain sizes on the SEM micrographs. The equivalent diameter of each grain was determined from the area measured. For each specimen, at least 300 grains were counted.

3. Results

The densification and shrinkage data of all the materials are shown in Figs 1 and 2 respectively. It is obvious that, among these materials, the one with the largest median grain size (material 2) was sintered to a lower density than the others and the powder with the narrowest size distribution (material 3) has the highest final density. From these plots, it can be seen that each curve appears to consist of two linear sections with different slopes. These linear sections were replotted separately and are shown in Fig. 3. From Fig. 3a, it

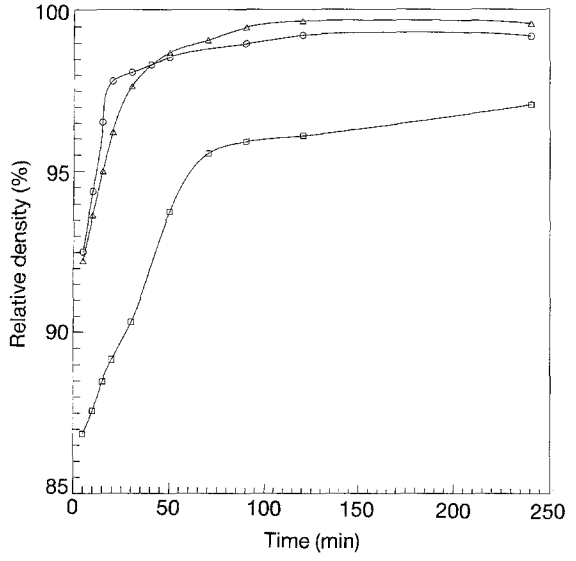

Figure 1 The densification curves for all the materials. ○—○, material 1; □—□, material 2; △—△, material 3.

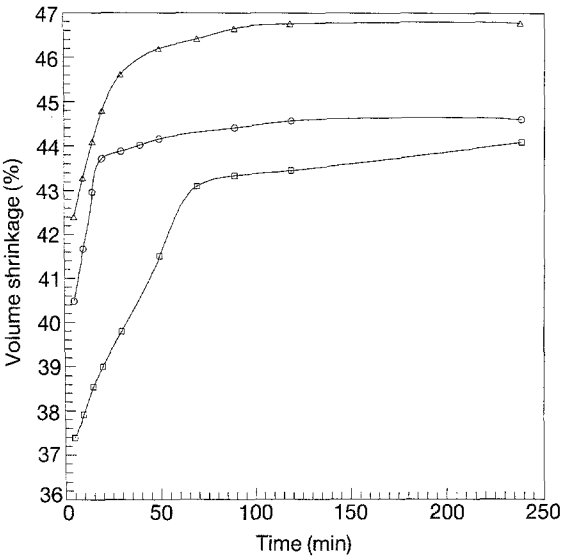

Figure 2 The volume shrinkage as a function of time for all the materials. ○—○, material 1; □—□, material 2; △—△, material 3.

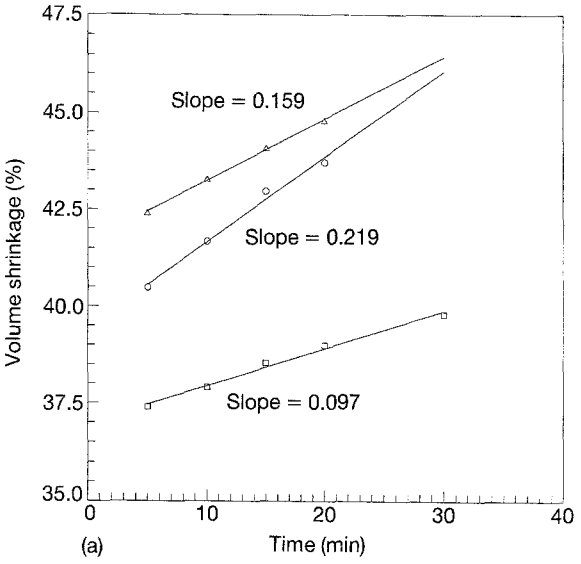

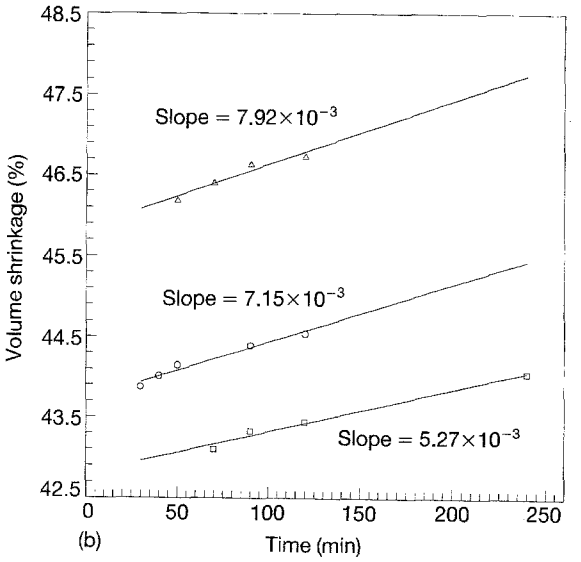

Figure 3a A plot showing the volume shrinkage rates prior to grain growth. (b) A plot showing the volume shrinkage rates after grain growth. ○—○, material 1; □—□, material 2; △—△, material 3.

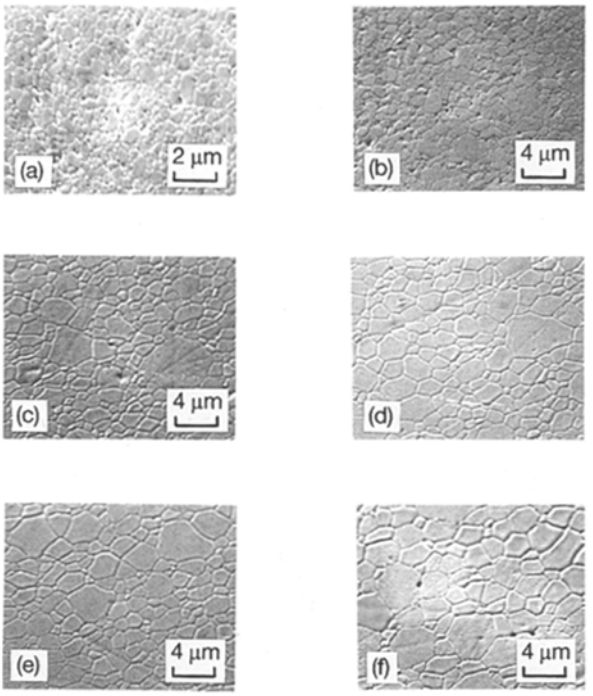

Figure 4 SEM micrographs of polished and etched specimens of material 1. The sintering times were 20, 30, 50, 90, 120, and 240 min for (a), (b), (c), (d), (e), and (f) respectively.

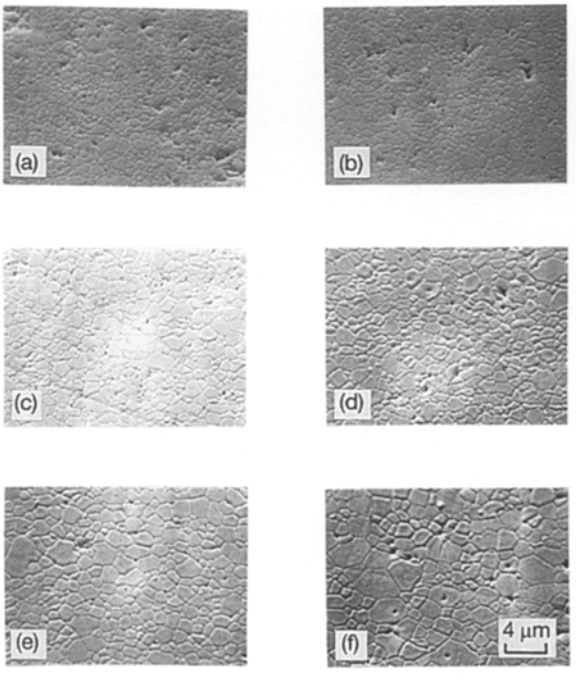

Figure 5 SEM micrographs of polished and etched specimens of material 2. The sintering times were 30, 50, 70, 90, 120, and 240 min for (a), (b), (c), (d), (e), and (f) respectively.

can be seen that material 1 has the highest shrinkage rate prior to the slope change and material 2 has the lowest shrinkage rate. However, after the change of slope material 3 has the highest shrinkage rate and material 2 still has the lowest shrinkage rate as shown in Fig. 3b.

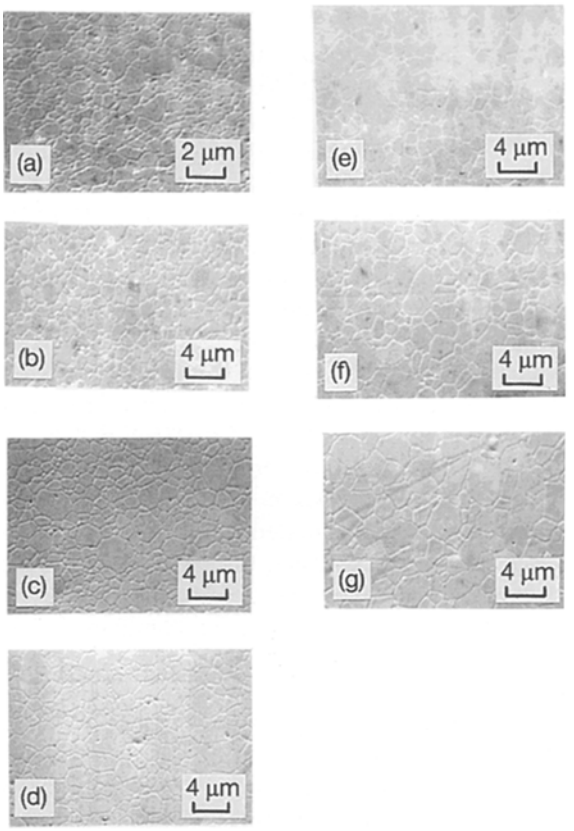

Figure 6 SEM micrographs of polished and etched specimens of material 3. The sintering times were 20, 30, 50, 70, 90, 120, 240 min for (a), (b), (c), (d), (e), (f), and (g) respectively.

The SEM micrographs reveal the microstructure of polished and etched specimens of all the materials; these are given in Figs 4–6. The grain size measurements performed on the etched specimens are shown in Figs 7–9. Both the cumulative distributions of the grain sizes measured (Figs 7a, 8a and 9a), and the curves characterized by log-normal distribution (Figs 7b, 8b and 9b), are included in these figures. Comparing the densification data and the grain size meassurements, one can find that the changes of the slopes correspond to the occurrence of grain growth. When the densification rate started to slow down, the average grain size started to increase. From the grain size measurements the grain growth kinetics were determined. Fig. 10 shows that the grain growth obeys the cubic law. It is apparent that finer grains with a narrower distribution width tend to grow more slowly.

4. Discussion

Both the model prediction [1] and the experimental results on the isothermal sintering of alumina indicate that sintering behaviours strongly depend on the starting particle size distribution. The width of the starting particle size distribution affects sintering kinetics in a similar manner to that prior to the occurrence of grain growth (hereinafter called phase I); the sintering rate increases and then decreases as the starting particle size distribution width increases. When

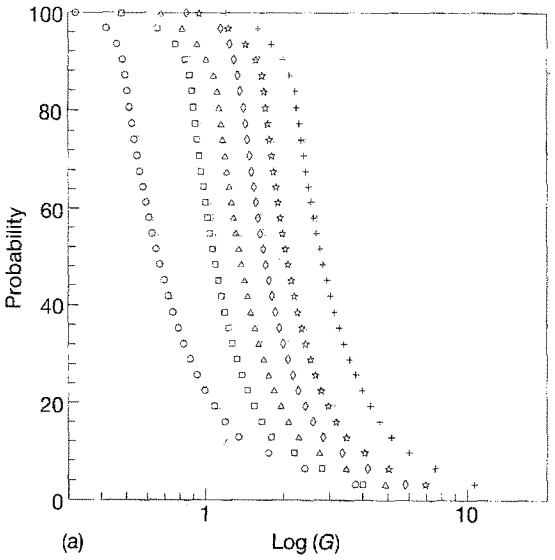

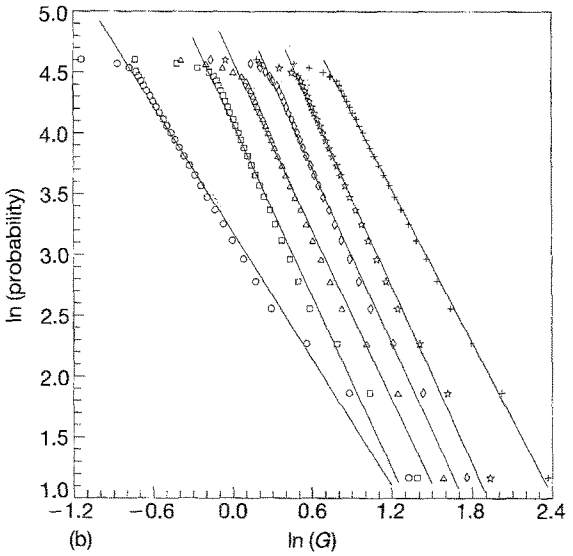

Figure 7a The cumulative grain size distributions of material 1 at various sintering times. (Every 10th data point is displayed). (b) The grain size distributions of material 1 characterized by log-normal distributions. (Every 10th data point is displayed) ○—○, 15 min; □—□, 25 min; △—△, 45 min; ◇—◇, 85 min; ☆—☆, 115 min; + — +, 235 min.

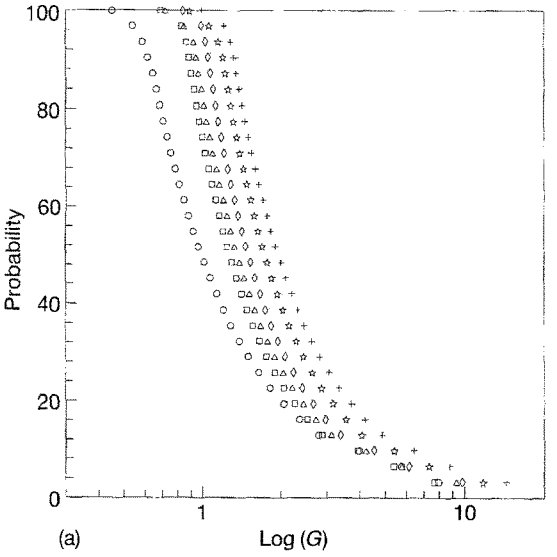

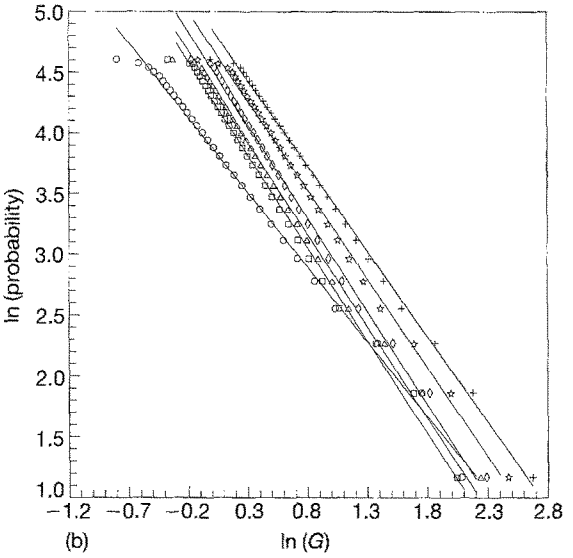

Figure 8a The cumulative grain size distributions of material 2 at various sintering times. (Every 10th data point is displayed.) (b) The grain size distributions of material 2 characterized by log-normal distributions. (Every 10th data point is displayed.) ○—○, 25 min; □—□, 45 min; △—△, 65 min; ◇—◇, 85 min; ☆—☆, 115 min; + — +, 235 min.

grain growth takes place (hereinafter called phase II), the sintering rate decreases as the width increases. It is noted here that, according to the model, the term *grain growth* means the growth of mean-size grain which is consistent with the definition commonly used. The experimental results indicate that at the end of phase I, the mean grain sizes of materials 1 and 3 exhibited minor growth. It can be regarded as a transition period. In fact, at the early stage of sintering, the very fine grains may grow [2] while the rest of the grains remain at the same size. This can be attributed to the rapid densification and the larger curvature of the fine powders.

4.1. Phase I

It can be seen from Figs 1 and 2 that after five minutes of sintering all the materials had proceeded into the intermediate stage. In the mean time, however, grain growth did not occur until the densification rates started to slow down as shown previously. Prior to the occurrence of grain growth, as shown in Fig. 3, the sintering rate is higher for powders with wider distribution or powders with smaller mean size. Appreciable grain growth was observed after 20 minutes of sintering for materials 1 and 3, and 30 minutes of sintering for material 2. It is noted that sintering of all the powders appears to be lattice diffusion controlled as the shrinkages were linearly proportional to time.

In order to relate the theoretical model and the experimental results, the constant K_1 in Equation 1 is evaluated. In the case of lattice diffusion-controlled sintering, K_1 can be expressed as [1]

$$K_1 = \frac{1}{(10^{-4})^3}(K_3\gamma\Omega D_l)\left(\frac{1}{kT}\right) \qquad (3)$$

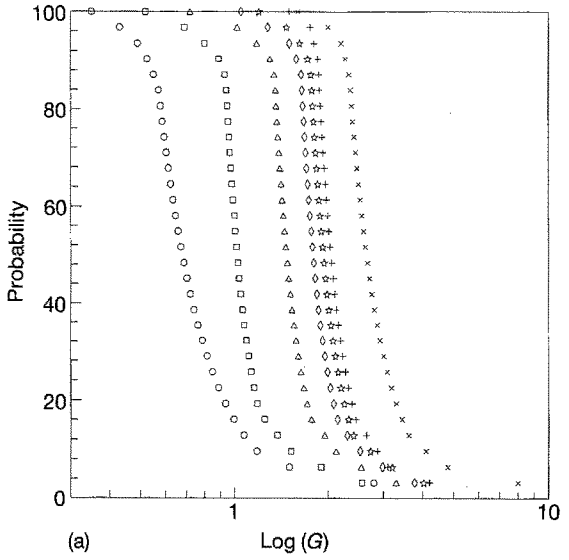

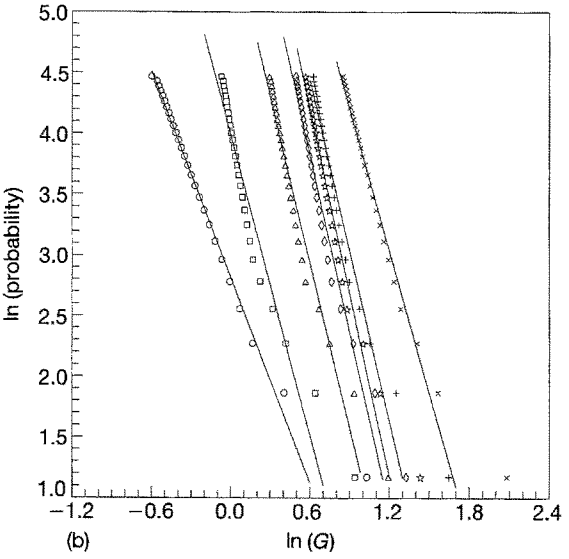

Figure 9a The cumulative grain size distributions of material 3 at various sintering times. (Every 10th data point is displayed.) (b) The grain size distributions of material 3 characterized by log-normal distributions. (Every 10th data point is displayed.) ○—○, 15 min; □—□, 25 min; △—△, 45 min; ◇—◇, 65 min; ☆—☆, 85 min; +—+, 115 min; ×—×, 235 min.

where K_3 is a constant and the first term on the right hand side is the conversion factor for the unit. In the modelling development, the unit of grain size was microns and has to be converted to centimetres here to be consistent with the units of other parameters. The numerical values from the literature [3–6] as given in Table II, are used to obtain the numerical value of K_1.

As a result, $K_1 = 2.65 \times 10^{-4}\,\text{min}^{-1}$. Therefore, in the case of lattice diffusion controlled for the intermediate stage of sintering prior to grain growth, the volume shrinkage can be expressed as

$$\frac{\Delta V}{V_0} = 2.65 \times 10^{-4} F_0 t \qquad (4)$$

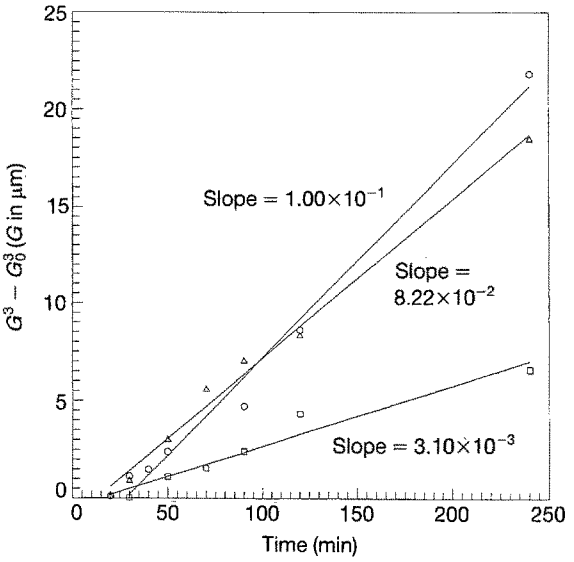

Figure 10 A plot showing the grain growth of all the materials obeying the cubic law. ○—○, 0.5 W; □—□, low; △—△, AS.

TABLE II Data used to calculate K_1 in Equation 3

K_3: 420	Ref. [3]
γ: 950 erg cm^{-2}	[4, 5]
Ω: 1.4×10^{-23} cm^3	[4]
D: 1.94×10^{-13} cm^2 s^{-1}	[6]

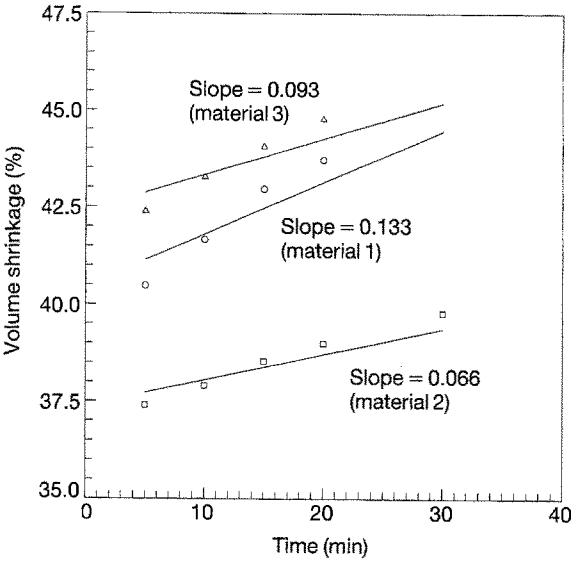

Figure 11 A comparison of experimental data with the theoretical model prior to grain growth. The solid lines represent the predictions from the modelling.

Taking the values of corresponding F_0 from the modelling [1], i.e. 422 for material 1, 184 for material 2, and 270 for material 3, the plots showing volume shrinkage versus time for all the materials are given in Fig. 11. To plot these curves, the initial volume shrinkage (occurred during the five-minute non-isothermal sintering) values of extrapolated experimental data have been used. It is noted that Equation 4 does not consider the shrinkage occurring during non-isothermal sintering. As shown in the figure, from both

the model prediction and the experimental results, material 1 has the highest rate (slope) and material 3 has the lowest rate. The experimental results also reveal the effect of mean particle size on the sintering kinetics. Larger mean sizes reduce sintering rate as predicted by classical sintering models and tend to diminish the effect of distribution width on sintering rate. This can be explained by the effect of agglomerates which act as large particles. Agglomerates can impede sintering rate [7] especially during the early time of sintering [8]. A reduction of sintering rate by as much as a factor of 10 was observed [9].

4.2. Phase II

To apply the model to the experimental data in this phase, an implicit assumption in the modelling has to be justified. The assumption was that the ratio of pore size to grain size favours pore shrinkage so that no pore coarsening occurs in this phase. The stability of a pore depends not only on the value of the dihedral angle but also on the number of surrounding grains. For a regular polyhedral pore surrounded by grains, the relation between its circumscribed sphere radius, r, and the radius of curvature of the pore surfaces, r_ρ, can be expressed as [10]

$$r_\rho = \frac{\sin\left(90^\circ - \frac{\phi_1}{2}\right)}{\sin\left(\frac{\phi}{2} - \frac{\phi_1}{2}\right)} r \tag{5}$$

where ϕ is the equilibrium dihedral angle and ϕ_1 is the dihedral angle of the polyhedron pore. There are conditions for the pore to be stable ($r/r_\rho = 0$), for the pore to shrink ($r/r_\rho > 0$), or for the pore to grow ($r/r_\rho < 0$). In this study, the microstructural examinations show that the pores are surrounded by three or four grains. This structure, as shown in Fig. 12, favours pore shrinkage and therefore the implicit assumption, i.e. pores will shrink, is justified.

The other assumption made in the modelling is the self-similar one of grain growth. It is found in this study that this is true in the period of grain growth. The results of image analysis show that before the average grain size started to increase, most of the submicron grains had already disappeared. On the other hand, these submicron grains might only be "invisible" to the image analyser due to its resolution. The grain size measurements indicate that when the

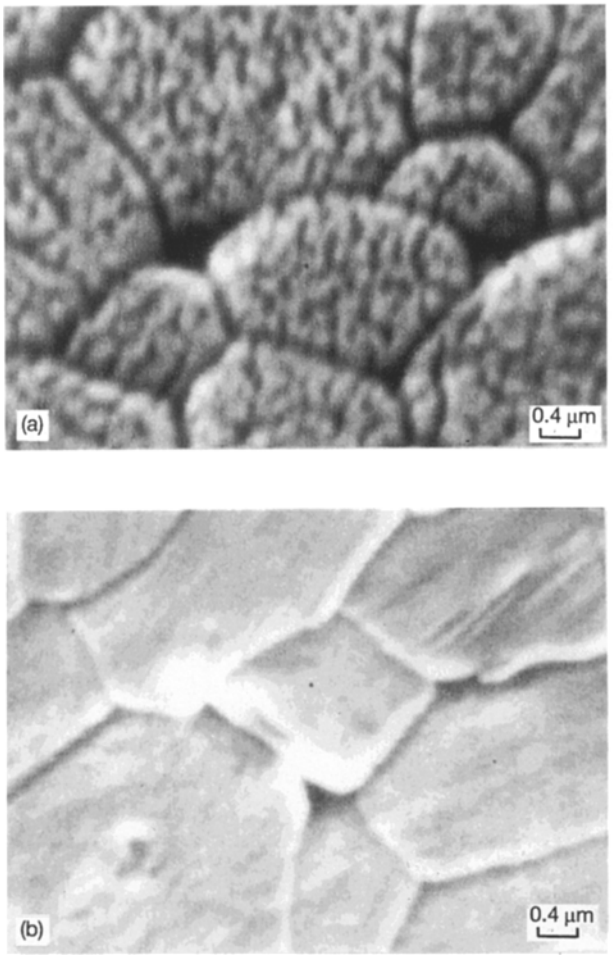

Figure 12a SEM micrographs showing the sintered structure for material 1. The sintering times were 30 and 50 min for (a) and (b) respectively.

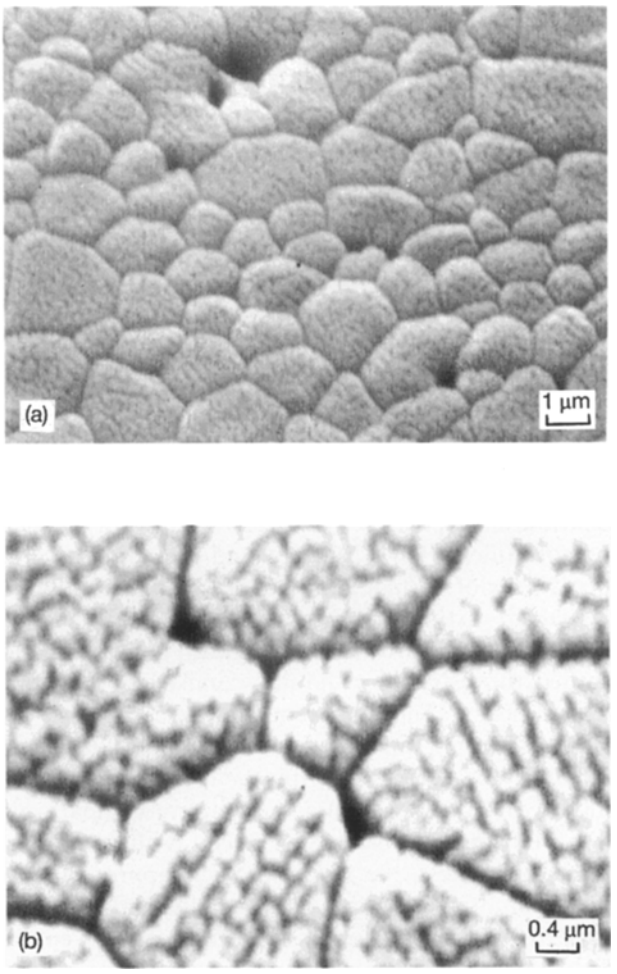

Figure 12b SEM micrographs showing the sintered structure for material 2. The sintering times were 30 and 120 min for (a) and (b) respectively.

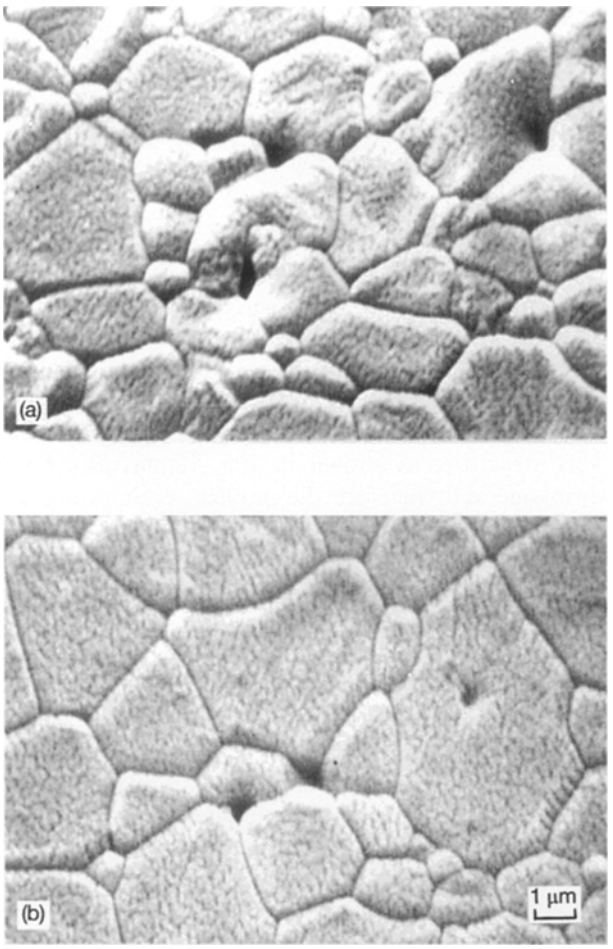

Figure 12c SEM micrographs showing the sintered structure for material 3. The sintering times were 50 and 90 minutes for (a) and (b) respectively.

TABLE III Numerical values of R, σ, and G_g

	Material 1	Material 2	Material 3
R	7.15×10^{-3}	5.27×10^{-3}	7.92×10^{-3}
σ	2.04	2.52	1.72
G_g	0.50	0.98	0.50

(mean) grain size started to increase, the grain size distribution decreased. This is consistent with the theory of Hillert [11] who suggested that prior to the occurrence of normal grain growth, a transition period which disturbs the size distribution may occur. However, as the growth of the (mean) grain size proceeded, the distribution did show similarities up to the occurrence of abnormal grain growth.

It was found that the experimental results were qualitatively consistent with the prediction of the model. In order to have a quantitative comparison, the following approach was taken. Within the size range of interest, the model predicts approximately a linear relationship between the $\ln(R)$ and $\ln[1/(\sigma G_g)]$. The experimental data are given in Table III. With these data are plotted, a linear relationship can be obtained as shown in Fig. 13.

Finally, the effect of particle size distribution on sintering behaviour is to be examined using the grain

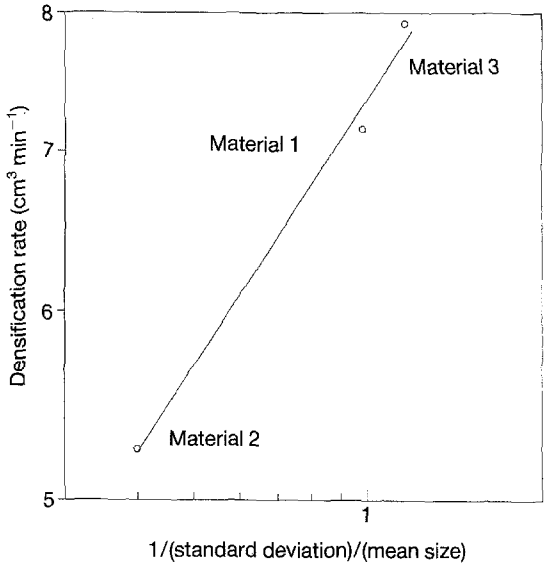

Figure 13 A plot showing the linear relationship between sintering rates and size distribution parameters are predicted by the model.

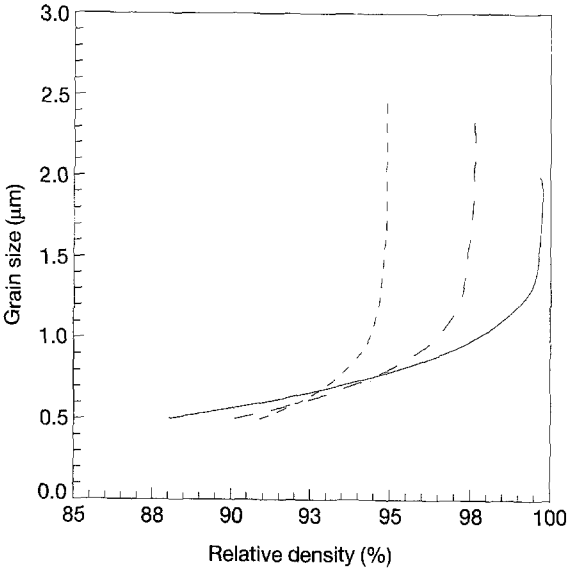

Figure 14 Grain size/density trajectories showing the effect of size distribution on sintering behaviour. (——) Standard deviation = 1.1; (— —) Standard deviation = 1.5; (– – –) Standard deviation = 2.0.

size/density trajectory. From the previous paper [1], the simplest form of $H(t)$ in Equation 2a is a linear function of time, i.e.,

$$H(t) = K_4 t \tag{6}$$

where K_4 is a constant. In addition, R in Equation 2 has previously been taken as the volume shrinkage. In the density range of interest (> 85%), it can be shown that the volume shrinkage is linearly proportional to the density, ρ. As a result, Equation 2 can be rewritten as

$$\rho \simeq K_5 F_1 t \tag{7}$$

where $K_5 = K_2 \times K_4$. In order to correlate the grain size and the density so that grain size/density trajectories can be constructed, the following equation

is used [12].

$$\frac{dG}{dt} = \frac{K_6}{G^2(1-\rho)} \tag{8}$$

where K_6 is a constant. Introducing Equation 7 into Equation 8, one has

$$\frac{G^2}{K_6} dG = \frac{dt}{(1 - K_5 F_1 t)} \tag{9}$$

Upon integrating and rearranging the above equation, one has

$$G^3 = G_0^3 \frac{3K_5}{K_4 F_1} \ln(1-\rho) - K_7 \tag{10}$$

where K_7 is a constant resulting from the integration. The above equation describes the relationship between grain size and density. This equation is employed to construct grain size/density trajectories.

To construct such plots, we have to determine the values of constants K_5, K_6, and K_7. Due to the lack of theoretical as well as experimental data in the literature, we will use the experimental data obtained in this study to determine these constants. Three distribution widths will be evaluated which are $\sigma_g = 1.1$, 1.5 and 2.0. From the previous analysis, it is known that $(K_5 \times F_1)$ can be determined using the experimental data shown. Similarly, one can determine the approximate value of K_6. The result is that $3K_6/K_5 \simeq 10^{-2}/(10^{-3}/10) = 100$. As mentioned earlier, K_7 is a constant resulting from the integration. It corresponds to time t when G maintains its original size and the density is equal to some value. Therefore K_7 will be determined while performing the numerical analysis. Another parameter needed is F_1. The values of F_1 corresponding to the distribution width given above are determined from the modelling. These values are $F_1 = 4.9$, 1.4, and 4.3 for $\sigma_g = 1.1$, 1.5, and 2.0 respectively.

Using these data, a sintering map showing the grain size/density trajectories of different systems with various distribution widths can be obtained. The plot is given in Fig. 14. The effect of powder size distribution on sintering at latter stages is shown in this figure. It can be seen that the one with the narrowest size distribution will sintered to the highest density and *vice versa.*

5. Conclusion

1. The sintering of alumina has been carried out at 1500 °C to test the model described previously. The experimental data prove that this model is applicable.

2. The grain size/density trajectory was applied to reveal the effect of grain size distribution on sintering behaviour. It shows that powders with the narrower size distribution sinter to the higher density and *vice versa.*

Acknowledgements

This work was supported by the Ohio Edison Program, Astro Met Associates, OH, USA and Applied Science, Inc. OH, USA.

References

1. J.-M. TING and R. Y. LIN "The Effect of Particle Size distribution on Sintering: Part I. Modelling", *J. Mater. Sci.* **29** (1994) 1867).
2. J. P. SMITH and G. L. MESSING, *J. Am. Ceram. Soc.* **67** [4] (1984) 238.
3. R. L. COBLE, *J. Appl. Phys.* **32** [5] (1961) 787.
4. R. L. COBLE, *J. Am. Ceram. Soc.* **41** [2] (1958) 55–62.
5. D. L. JOHNSON and I. V. CULTER, *J. Am. Ceram. Soc.* **46** [11] (1963) 545.
6. R. L. COBLE, *J. Appl. Phys.* **32** [5] (1961) 793.
7. M. D. SACK and J. A. PASK, *J. Am. Ceram. Soc.* **65** [2] (1982) 70.
8. W. H. RHODES, *J. Am. Ceram. Soc.* **64** [1] (1981) 19–22.
9. F. W. DYNYS and J. W. HALLORAN, *J. Am. Ceram. Soc.* **67** [9] (1984) 596.
10. W. D. KINGERY and B. FRANKOIS, in "Sintering and related phenomena", edited by G. C. Kuczynski, N. A. Hooten, and C. F. Gibbon (Gordon and Breach, New York 1967, pp. 471–98.
11. M. HILLERT, *Acta Met.* **13 March** (1965) 227.
12. K. A. BERRY and M. P. HARMER, *J. Am. Ceram. Soc.* **69** [2] (1986) 143.

Received 13 October 1993
and accepted 5 July 1994